



A dimeric polyoxometalate sandwich motif containing a truncated $\{Mn_3O_4\}$ cubane core

Scott G. Mitchell, Haralampos N. Miras, De-Liang Long, Leroy Cronin*

WestCHEM, School of Chemistry, Joseph Black Building, University of Glasgow, University Avenue, Glasgow G12 8QQ, UK

ARTICLE INFO

Article history:

Available online 17 July 2010

Dedicated to Prof. Achim Müller and his continuing contributions to chemistry

Keywords:

Polyoxometalates
Silicotungstate
Lacunary Keggin
Cubane core
Self assembly
Crystallography

ABSTRACT

A novel sandwich-type silicotungstate motif, $K_{18}[Mn^{II}_2\{Mn^{II}(H_2O)_5Mn^{III}_3(H_2O)(B-\beta-SiW_9O_{34})(B-\beta-SiW_6O_{26})\}_2] \cdot 20H_2O$ **1**, has been isolated from the reaction of $K_8[\gamma-SiW_{10}O_{36}] \cdot 12H_2O$ and manganese ions in aqueous acidic media. The transition metal-substituted polyoxometalate (TMSP) **1** has been fully characterized by single-crystal X-ray diffraction, elemental analysis, thermogravimetric analysis, and infrared spectroscopy. This dimeric polyanion consists structurally of the sandwich polyanion $\{Mn^{II}(H_2O)_5Mn^{III}_3-(H_2O)(B-\beta-SiW_9O_{34})(B-\beta-SiW_6O_{26})\}$, dimerized via two manganese(II) linker ions. Each monomeric unit is composed of two non-equivalent Keggin fragments, $(B-\beta-SiW_8O_{31})$ and $(B-\beta-SiW_6O_{26})$, linked to each other via three manganese ions resulting in a truncated $\{Mn_3O_4\}$ cubane core. Experimental, structural, and electrochemical aspects of the material are reported and discussed.

© 2010 Elsevier B.V. All rights reserved.

1. Introduction

Polyoxometalates (POMs) represent a vast class of molecular, anionic metal-oxide clusters of early *d*-block transition metals in high oxidation state (e.g. W^{VI} , Mo^{VI} , and V^V) [1,2]. Edge- and corner-shared MO_6 octahedra link together to form discrete clusters with such diversity in size, shape, charge density, redox potentials, and solubility that these materials possess a virtually unrivaled range of topologies with tunable physical and chemical properties [3,4]. Consequently, POMs have attracted increased attention in recent years and have been screened for application in areas such as biology [5], magnetism [6], materials science [7] and but by far their greatest application is as industrial catalysts [8]. Although these polyanionic species have been known for almost two centuries, many new members of this unique class of metal-oxide clusters with unexpected shapes and versatile topology are still being discovered, resulting in enormous diversity in size, shape, and application [9,10].

Abbreviations: aq, aqueous; conc, concentrated; eq, equivalent; FT-IR, Fourier transformation infra-red; FAAS, flame atomic absorption spectrometry; FP, flame photometry; HPOM, heteropolyoxometalate; JT, Jahn-Teller; POM, polyoxometalate; TGA, thermogravimetric analysis; TMSP, transition metal-substituted polyoxometalate; UV-Vis, ultraviolet-visible; XRD, X-ray diffractometry.

* Corresponding author. Tel.: +44 141 330 6650; fax: +44 141 330 4888.

E-mail address: L.Cronin@chem.gla.ac.uk (L. Cronin).

URL: <http://www.croninlab.com> (L. Cronin).

One POM sub-class of particular interest in recent years has been the transition metal-substituted polyoxometalates (TMSPs). These metal-oxides represent an attractive system to work towards the grand aim of real design, owing to their relatively simple preparation and manipulation; not to mention the many interesting properties they exhibit. As a result, these derivatives have been the subject of a vast number of reports in the last decade [11,12]. The identification and isolation of discrete building blocks to produce versatile and modular species that can be assembled in a controlled manner still represents a fundamental objective in the discipline of inorganic chemistry. For the polyoxometalates, the most fruitful and widespread method employed to yield novel or closely-related cluster fragments and architectures is by carefully screening and controlling the reaction conditions [13]. One common synthetic strategy employed to obtain TMSPs involves the reaction of a preformed lacunary POM (i.e. one containing addenda atom structural vacancies) with a transition metal in a one-pot procedure.

For the polyoxotungstates in particular, many well-defined lacunary species are known; each possessing its own reactivity and stability trend, therefore synthetically, special attention is paid to fine changes in reaction conditions such as pH, temperature, buffer capacity, ionic strength, and cation size: all having the potential to exert a considerable effect on the polyanion equilibria and formation of products [14]. A lacunary polyanion of particular versatility is the divacant silicodectatungstate $[\gamma-SiW_{10}O_{36}]^{8-}$ [15], which has variable stability in aqueous media, and is observed to undergo structural transformations at both low and high pH [13]. The

incorporation of TMs into POMs has introduced centres of magnetic or catalytic potential into discrete structures thereby facilitating access to an even broader range of functional materials. An abundance of transition metal containing clusters exists in the recent literature; however, Mn-based aggregates are much rarer. The surprising scarcity of inorganic ligand-based Mn clusters may be partially attributed to the lack of easy access to coordinatively flexible inorganic ligands upon which polynuclear manganese clusters can be constructed. Furthermore, antiferromagnetic interactions between manganese spin centres often result from monoatomic bridging modes of O^{2-} or OH^- groups when inorganic ligand units are used alone, thereby limiting the generation of high-spin ground state species (e.g. Mn^{II} (d^5), Mn^{III} (d^4), Mn^{IV} (d^3)). Many Mn-based molecules exhibit large ground spin states (S) and this, coupled with a large zero-field splitting parameter (D) derived from the single-ion anisotropy of Mn^{III} , give rise to the SMM behavior so well described in the current literature [16,17].

Of particular interest are the numerous sandwich-type polyoxoanions that have been synthesized: most motifs belonging to the well-known Weakley- [18], Hervé- [19], Krebs- [20], and Knoth-type [21] sandwich structures. Since these structures possess a larger volume and negative charge than either lacunary or fully filled polyoxotungstates, they act as excellent precursors towards constructing both extended and functional materials. In 2009 we described the first 2D hybrid network constructed from sandwich $[Mn_4(PW_9O_{34})_2]^{10-}$ clusters [22] while Yang et al. synthesized several 2D frameworks made up of the M_4 -sandwiched polyoxotungstates under hydrothermal conditions [23]. More recently, the first polyoxometalate single molecule magnet $\{[XW_9O_{34}]_2[Mn^{III}_4Mn^{II}_2O_4(H_2O)_4]\}^{12-}$ composed of a mixed valence manganese double cubane core ligated by two polyanion ligand was reported by us [6]. Since then several other groups have reported single molecule magnet behaviour for POMs, such as mononuclear lanthanide SMMs $[Ln(W_5O_{18})_2]^{9-}$ [24]. The Kortz group have studied and obtained several examples of the M_3 - [14,25] and M_4 -sandwich-type polyoxotungstates [26].

Since the publication of our $Mn^{III}_4Mn^{II}_2$ -POM SMM complex [6], and Mn^{III} -Keggin Network [27] we have been exploring in great detail the reactivity of POMs with various magnetically interesting species from transition metals and other electrophiles to organometallic groups. The ligation of redox-active and potentially magnetic polyoxoanions doubtlessly adds an important control parameter to the magnetic properties of polynuclear manganese complexes, although interest in the research and exploration of inorganic Mn species stems also from their biological relevance: Mn is prominent in the active sites of many metalloenzymes [28,29] and a $\{Mn_3CaO_4\}$ cubane has been recently proposed for the catalytic site of the Oxygen-Evolving-Complex (OEC) of Photosystem II [30]. Regarding the oxidative properties of POMs and their use as catalysts, Hill and co-workers have had a great deal of success in recent years, particularly in determining the key properties of the water oxidation catalyst $Rb_8K_2\{[Ru^{IV}_4O_4(OH)_2(H_2O)_4](\gamma-SiW_{10}O_{36})_2\}$ [31] and more recently, with a POM complex comprising a $\{Co_4O_4\}$ core, $[Co_4(H_2O)_2(PW_9O_{34})_2]^{10-}$, which also acts as a hydrolytically and oxidatively stable homogeneous water oxidation catalyst [32]. In this article we report one of our initial findings on research into the coupling of dilacunary POMs with manganese ions with a view towards the design of functional inorganic materials.

2. Results and discussion

The formation of dimeric sandwich-type silicotungstate $[Mn^{II}_2\{Mn^{II}(H_2O)_5Mn^{III}_3(H_2O)(B-\beta-SiW_9O_{34})(B-\beta-SiW_6O_{26})_2\}]^{18-}$ **1a** is realized from the reaction of the dilacunary polyanion $[\gamma-SiW_{10}O_{36}]^{8-}$ with manganese complex $[Mn_3O(OAc)_6(py)_3]^{py}$

in the ratio of 1:1 in 0.1 M nitric acid (pH 2.0) at room temperature. Following the relatively short reaction period of approximately 30 min, one equivalent of potassium chloride was added to the reaction mixture to assist the isolation of the product by hastening its crystallization from solution, which began 7–10 days thereafter. Thus, polyanion **1** was crystallized as a pure potassium salt with twenty solvent water molecules associated with each cluster. The complete molecular formula of **1** is $K_{18}[Mn^{II}_2\{Mn^{II}(H_2O)_5Mn^{III}_3(-H_2O)(B-\beta-SiW_9O_{34})(B-\beta-SiW_6O_{26})_2\}] \cdot 20H_2O$, and is, to the best of our knowledge, a new polyoxometalate motif (Figs. 1 and 2).

The principle unit of dimeric **1a** is a sandwich polyanion composed of two non-equivalent Keggin units, $\{B-\beta-SiW_9O_{34}\}$ and $\{B-\beta-SiW_6O_{26}\}$. These two lacunary Keggin fragments are fused by three Jahn–Teller (JT) distorted octahedral manganese(III) ions; and connected into the dimer *via* two manganese(II) linker ions. Consequently, each monomeric unit of **1a** contains a truncated $\{Mn_3O_4\}$ cubane core. These incomplete cubanes consist of three Mn(III) centres with two μ_3-O^{2-} anions and two μ_2-O^{2-} anions acting as ligands. Furthermore, attached to the ‘rear-side’ of each $\{B-\beta-SiW_9O_{34}\}$ fragment is a Mn(II) ion with five coordinated water ligands. The oxidation state of the manganese ions were determined *via* bond valence sum analysis (BVS) in combination with the redox properties of the material. Dimeric $\{M_3(B-\beta-SiW_9O_{34})(B-\beta-SiW_6O_{31})\}$ sandwich polyanions are not new [13,14]; however, the novel nature of **1** arises principally from the substitution of the $\{B-\beta-SiW_8O_{31}\}$ fragment where two tungsten centres have been replaced by two manganese ions leading to a $\{B-\beta-SiW_6Mn^{III}_2O_{31}\}$ unit. Important for the formation of the dimeric sandwich structure of **1** is that the manganese(III) linker ions, Mn1, edge share μ_3-O^{2-} O46 with each other as well as the Si2 heteroatom of the $\{B-\beta-SiW_6O_{26}\}$ unit; but also corner share μ_2-O^{2-} atoms with tung-

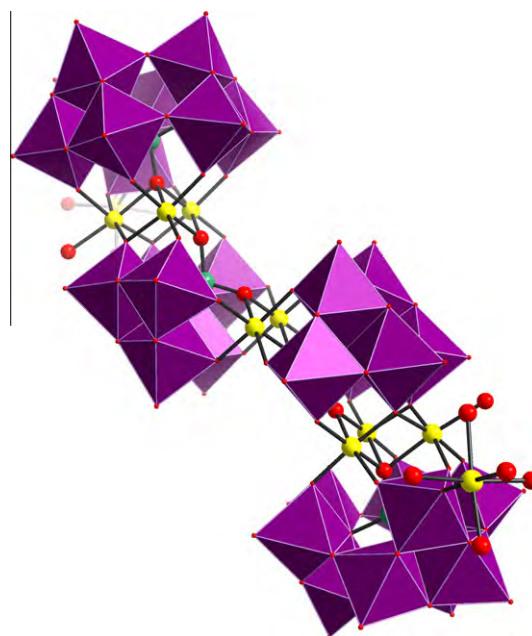


Fig. 1. Combined ball-and-stick/polyhedral representation of dimeric sandwich polyanion $[Mn^{II}_2\{Mn^{II}(H_2O)_5Mn^{III}_3(H_2O)(B-\beta-SiW_9O_{34})(B-\beta-SiW_6O_{26})_2\}]^{18-}$ **1a**. The monomeric building units of **1a** are each composed of two non-equivalent Keggin fragments $\{B-\beta-SiW_9O_{34}\}$ and $\{B-\beta-SiW_6O_{26}\}$ which are held together by three manganese(III) ions; and connected into the dimer *via* two manganese(II) linker ions. Attached to the ‘rear-side’ of each $\{B-\beta-SiW_9O_{34}\}$ unit is a $Mn^{II}O(OH)_2_5$ fragment so that the overall symmetry of the molecule is C_1 . Colour scheme: WO_6 (purple polyhedra); manganese (yellow spheres); silicon (green spheres) and oxygen (red spheres). All cations and solvent water molecules have been omitted for clarity. (For interpretation of the references to colour in this figure legend, the reader is referred to the web version of this article.)

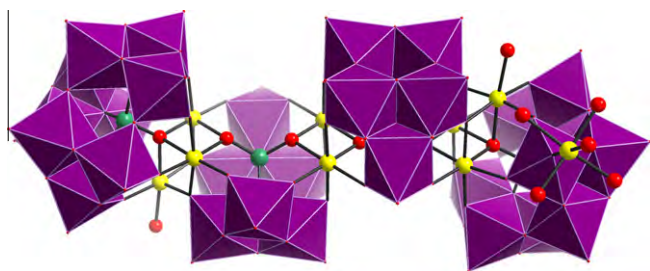


Fig. 2. Combined ball-and-stick/polyhedral representation of dimeric polyanion $[\text{Mn}^{\text{II}}_2[\text{Mn}^{\text{III}}(\text{H}_2\text{O})_5\text{Mn}^{\text{III}}_3(\text{H}_2\text{O})(\text{B}-\beta\text{-SiW}_9\text{O}_{34})(\text{B}-\beta\text{-SiW}_6\text{O}_{26})_2]^{18-}$ **1a** viewed from above. The non-equivalent Keggin building units of **1a** $\{\text{B}-\beta\text{-SiW}_9\text{O}_{34}\}$ and $\{\text{B}-\beta\text{-SiW}_6\text{O}_{26}\}$ and their connectivity to manganese ions can clearly be observed. Colour scheme: WO_6 (purple polyhedra); manganese (yellow spheres); silicon (green spheres) and oxygen (red spheres). All cations and solvent water molecules have been omitted for clarity. (For interpretation of the references to colour in this figure legend, the reader is referred to the web version of this article.)

sten atoms W1, W2, W4, and W5 of the $\{\text{B}-\beta\text{-SiW}_6\text{O}_{26}\}$ unit (see Figs. 1 and 2).

In the monomeric unit, each Keggin fragment in **1a** is linked to three Jahn–Teller distorted octahedral Mn(III) ions. The Mn ions are linked to each of the lacunary units *via* two Mn–O–W bonds and the two structurally equivalent Mn ions are also linked to an oxygen atom of each SiO_4 heteroatom group. In addition, these linking Mn(II) ions complete their octahedral coordination geometry by sharing an oxygen atom from each SiO_4 group. Although the exact mechanism of assembly of this molecule is not known, both silico-tungstate fragments in **1** must be formed by the decomposition of $[\gamma\text{-SiW}_{10}\text{O}_{36}]^{8-}$ *via* loss of tungsten octahedra, resulting first in $\{\text{B}-\beta\text{-SiW}_9\text{O}_{34}\}$ and then $\{\text{B}-\beta\text{-SiW}_6\text{O}_{26}\}$. Such decomposition pathways have been proposed for $[\gamma\text{-SiW}_{10}\text{O}_{36}]^{8-}$ and $[\gamma\text{-GeW}_{10}\text{O}_{36}]^{8-}$ [14]. Following decomposition, it is likely that insertion of manganese ions occurs; possibly resulting in the monomeric fragment $\{\text{Mn}^{\text{II}}(\text{H}_2\text{O})_5\text{Mn}^{\text{III}}_3(\text{H}_2\text{O})(\text{B}-\beta\text{-SiW}_9\text{O}_{34})(\text{B}-\beta\text{-SiW}_6\text{O}_{26})\}$ followed by addition of the Mn(II) linker ions leading to dimerization which stabilized the monomeric fragment and thus yields compound **1**. Of course, at this stage, such mechanistic information is merely speculative and formation can only formally be described as ‘self-assembly’ from aqueous solution.

The truncated $\{\text{Mn}_3\text{O}_4\}$ cubane core located between the $\{\text{B}-\beta\text{-SiW}_9\text{O}_{34}\}$ and $\{\text{B}-\beta\text{-SiW}_6\text{O}_{26}\}$ fragments is illustrated by Fig. 3. The electron configurations, and hence coordination geometries,

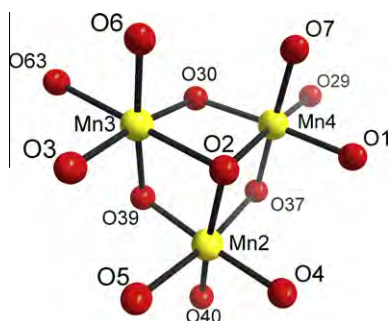


Fig. 3. Isolated core unit of $[\text{Mn}^{\text{II}}_2[\text{Mn}^{\text{III}}(\text{H}_2\text{O})_5\text{Mn}^{\text{III}}_3(\text{H}_2\text{O})(\text{B}-\beta\text{-SiW}_9\text{O}_{34})(\text{B}-\beta\text{-SiW}_6\text{O}_{26})_2]^{18-}$ **1a** showing the truncated cubane core which is composed of three high-spin Jahn–Teller (JT) distorted Mn(III) centres bound by $\mu_2\text{-O}^{2-}$ and $\mu_3\text{-O}^{2-}$ anions. All Mn(III) ions are d^4 and six-coordinate: Mn2 is ligated to six oxo-ligands (three $\mu_2\text{-O}^{2-}$, two $\mu_3\text{-O}^{2-}$ and one $\mu_4\text{-O}^{2-}$), Mn3 is ligated to five oxo-ligands (two $\mu_2\text{-O}^{2-}$, two $\mu_3\text{-O}^{2-}$ and one $\mu_4\text{-O}^{2-}$) plus one H_2O ligand: $\text{Mn}^{\text{II}}\text{O}_5(\text{OH}_2)$; while Mn4 is coordinated to six oxo-ligands (three $\mu_2\text{-O}^{2-}$ and two $\mu_3\text{-O}^{2-}$ and one $\mu_4\text{-O}^{2-}$). All three Mn ions share O2, which is $\mu_4\text{-O}^{2-}$ and bound also to Si. Colour scheme: manganese (yellow spheres) and oxygen (red spheres). (For interpretation of the references to colour in this figure legend, the reader is referred to the web version of this article.)

of the three Mn(III) centres (high-spin d^4) result in Jahn–Teller (JT) distorted geometries. In this instance, the distortion produces axially elongated octahedral coordination along their z-axes, which gives rise to elongated Mn–ligand bonds. The JT axis of the manganese ion Mn2 lies along the line from the oxygen of the $\mu_3\text{-oxide}$ O39 in the cube to the water oxygen atom O(4) from the Mn(2) atom. The JT axis of the Mn(3) ion, which is along O(2)–Mn(3)–O(63), is parallel to that of Mn(2), with the Mn–O bond lengths averaging 2.23 ± 0.01 Å at an angle of 174.5° to one another. While for the Mn4 ion, this lies along O(2)–Mn(4)–O(29). Closer inspection of the Mn–O bond lengths in **1** indicates that the equatorial bonds are in the normal range (Mn(2)– O_{eq} 1.924 ± 0.04 Å, Mn(3)– O_{eq} 1.931 ± 0.01 Å, and Mn(4)– O_{eq} 1.933 ± 0.04 Å). As expected, the axial Mn–O bonds are longer and actually fall into categories of long and very long for each manganese (Mn2– O_{ax} $2.112(9)$, $2.283(8)$ Å; Mn(3)– O_{ax} $2.218(8)$, $2.240(8)$ Å; and Mn(4)– O_{ax} $2.048(8)$, $2.254(8)$ Å) (see Fig. 3 in conjunction with Table 2). The Mn··Mn distances in the $\{\text{Mn}_3\text{O}_4\}$ cubane are in the range of $3.050(2)$ – $3.161(5)$ Å. The longest distance of $3.161(5)$ Å is found between the Mn3–Mn(4) pair which are bridged by one $\mu_3\text{-O}^{2-}$ with an Mn(3)–O(30)–Mn(4) angle of 107.02° and one $\mu_4\text{-O}^{2-}$ ion with angle Mn(3)–O(2)–Mn(4) equal to 90.32° . The remaining Mn··Mn pair of Mn(II) ions (Mn1), which bridge and link together the two sandwich clusters, are at a distance of $3.100(1)$ Å from each other and have a Mn(1)–O(46)–Mn(1) separation angle of 95° .

There are several key packing forces and crystal symmetry which determine the chemical and physical properties of **1**. The highly symmetrical ions contained within the molecule transfer their symmetry to the cluster. Consequently, under the crystallization conditions employed, molecules of **1** crystallize in the monoclinic space group $P2_1/c$, the unit cell of which can be viewed in Fig. 4. The presence of potassium is vital to the stability of single crystals of **1** and it is principally the abundance of these relatively weak interactions which hold individual molecules together (see Fig. 4).

The redox behaviour of the compound **1** was studied in aqueous solution. Fig. 5 shows the main characteristic peaks associated with W and Mn redox couples of compound **1** between $+2.000$ V and -1.000 V versus Ag/AgCl at the scan rate region of 50 mV s^{-1} . The form of the diagram remained identical independent on the scanning potential direction, indicating that the phenomena observed in one domain had a negligible influence on those in the other domain. At this scan rate and scanning towards the negative region of potential values, the reduction of W centres occurs through two separated steps, with the corresponding $E_{1/2}$ peak potentials located at -0.260 and -0.385 V, respectively (versus Ag/AgCl) and are in agreement with previous reported examples even though minor differences in potential locations are observed; in some cases this depends on the ionic strength and the pH value of the medium [34,35]. At the positive region of potential values two overlapping oxidation peaks observed with the E peak potential to be located at $+1.046$ and $+1.416$ V. The simultaneous oxidation of all Mn(II) centres can also be observed in the voltammograms, followed by an oxidation of Mn(III) centres to Mn(IV) accompanied by the absorption of active species on the surface of the electrode. Furthermore, these are in good agreement with previously reported Mn–POM compounds [36]. Various cases were described in the literature for the oxidation pathways of Mn centers within POMs, with a variety of situations, including important differences in potential locations [37]. The reduction process takes place in two well separated steps with the peaks located at $+0.728$ and $+1.112$ V. The cyclic voltammograms of **1** at different scan rates showed that the peak currents were proportional to the scan rate, indicating that redox processes of **1** are surface-controlled when the scan rate does not exceed a rate of 50 mV s^{-1} . Above 100 mV s^{-1} the peak currents were proportional to the square root of the scan rate, suggesting that the redox process is

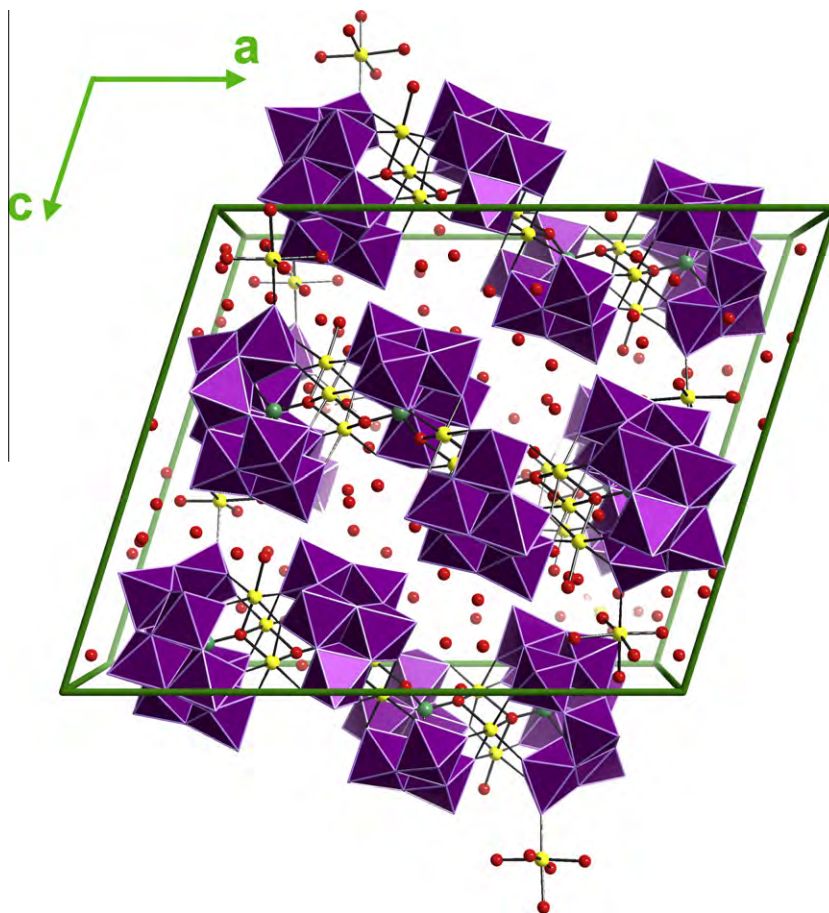


Fig. 4. Packing of **1a** along the crystallographic *b*-axis. Potassium ions have been removed for clarity; however, solvent water molecules (isolated red spheres) have been retained to illustrate packing of the crystal structure. Green box: unit cell. Colour scheme: WO_6 (purple polyhedra); manganese (yellow spheres); silicon (green spheres) and oxygen (red spheres). (For interpretation of the references to colour in this figure legend, the reader is referred to the web version of this article.)

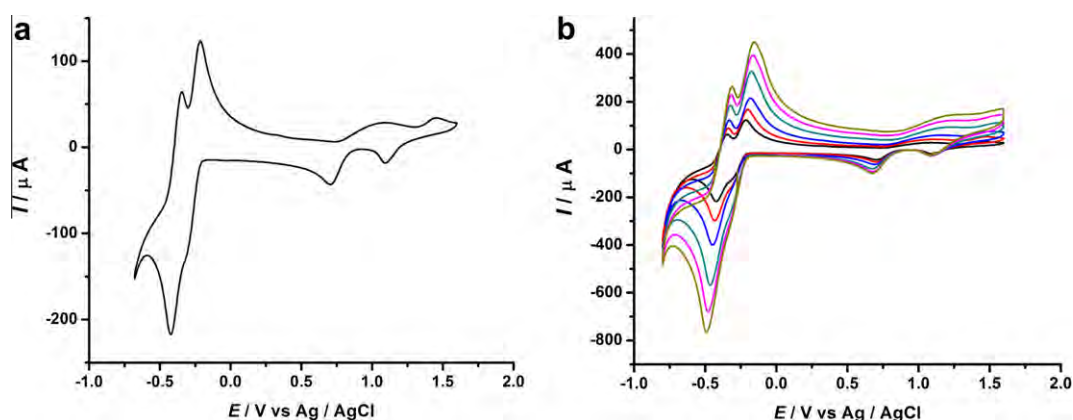


Fig. 5. (a) Cyclic voltammogram of compound **1** (10^{-3} M) in 10 mL of 0.2 M Na_2SO_4 in 0.1 M $\text{CH}_3\text{COONa}/\text{CH}_3\text{COOH}$ buffer solution at a scan rate of 50 mV s^{-1} ; (b) Cyclic voltammograms of **1** at scan rates (from inner to outer) 25, 50, 100, 200, 300, and 400 mV/s . The working electrode was glassy carbon (1.5 mm) and the reference electrode was Ag/AgCl and CV studies were carried out at room temperature of 18°C .

diffusion-controlled. Upon exceeding a scan rate of 100 mV s^{-1} , broadening and overlapping of the redox couples was observed and as a consequence important redox-related information was concealed.

3. Conclusions

In summary, a new dimeric mixed-valence manganese-substituted silicotungstate polyanion – $\text{K}_{18}[\text{Mn}^{\text{II}}_2\{\text{Mn}^{\text{II}}(\text{H}_2\text{O})_5\text{Mn}^{\text{III}}_3$

$(\text{H}_2\text{O})(\text{B}-\beta\text{-SiW}_9\text{O}_{34})(\text{B}-\beta\text{-SiW}_6\text{O}_{26})_2\} \cdot 20\text{H}_2\text{O}$ **1** has been synthesized and fully characterized. The electrochemical properties have been studied by cyclic voltammetry showing the main characteristic peaks associated with W and Mn redox couples of the polyanion. The synthesis of this compound represents one of the many possible one-pot procedures by which we can incorporate mixed-valence transition metal centres into the truncated cubane core of $\{\text{M}_3\}$ -type sandwich TMSPs. Furthermore, the synthetic procedure involved in producing **1** employs the dilacunary polyanion

$[\gamma\text{-SiW}_{10}\text{O}_{36}]^{8-}$ and serves as a testament to the versatility of this particular fragment as a starting material for molecules designed to meet a specific functional requirement, such as water oxidation catalysts or single molecule magnets. The presence of several paramagnetic transition metal ions with high-spin ground states in close proximity leads to the possibility of exchange-coupled spins and consequently, future work must certainly focus on in-depth studies into the magnetic properties of this compound, and related compounds that we attempt to engineer for purposes of comparison and attempting the systematic control of structure and function.

4. Experimental

4.1. Materials

All reagents and chemicals were supplied by Sigma–Aldrich Chemical Company Ltd., and Riedel-de-Haën and were used without further purification. Solvents were supplied by Fisher Chemicals. $\text{K}_8[\gamma\text{-SiW}_{10}\text{O}_{36}]\cdot 12\text{H}_2\text{O}$ was prepared using the published procedure [33].

4.2. Instrumentation

4.2.1. Fourier-transform infrared (FT-IR) spectroscopy

The compound was prepared as a KBr pellet and FT-IR spectra were collected in transmission mode using a JASCO FT-IR-410 spectrometer. Wavenumbers ($\tilde{\nu}$) are given in cm^{-1} ; intensities as denoted as vs = very strong, s = strong, m = medium, w = weak, br = broad, sh = sharp.

4.2.2. Microanalysis

Carbon, nitrogen, and hydrogen content were determined by the microanalysis services within the Department of Chemistry, University of Glasgow using a EA 1110 CHNS, CE-440 Elemental Analyser.

4.2.3. Single crystal X-ray diffraction

Single crystal datasets were collected at 150(2) K on an Oxford Diffraction Gemini Ultra ($\lambda(\text{Mo K}\alpha) = 0.71073 \text{ \AA}$) equipped with a graphite monochromator and ATLAS CCD detector.

4.2.4. UV–Vis spectroscopy

UV–Vis spectra were collected using a Shimadzu PharmaSpec UV-1700 UV–Vis spectrophotometer in transmission mode using quartz cuvettes with 1.0 cm optical path length.

4.2.5. Thermogravimetric analysis (TGA)

Thermogravimetric analysis was performed on a TA Instruments Q 500 Thermogravimetric Analyzer under nitrogen or air flow at a typical heating rate of either $5 \text{ }^\circ\text{C min}^{-1}$ or the initial heating range was from room temperature to $150 \text{ }^\circ\text{C}$ at $2 \text{ }^\circ\text{C per min}$ followed by a second range from $150 \text{ }^\circ\text{C}$ to $1000 \text{ }^\circ\text{C}$ at $5 \text{ }^\circ\text{C per min}$.

4.2.6. Flame atomic absorption spectroscopy analysis

FAAS analysis for W and Mn content was performed at the Environmental Chemistry Section, Department of Chemistry, The University of Glasgow on a Perkin–Elmer A Analyst 400 atomic absorption spectrophotometer.

4.2.7. Flame photometry

K and Na content were measured using a Corning flame photometer 410.

4.2.8. Electrochemistry

Voltammograms were obtained using a Voltalab model GPZ 301 electro analysis system. The standard three-electrode arrangement was employed with a Pt mesh auxiliary electrode, 3 mm glassy carbon working electrode, and Ag/AgCl reference electrode. All potentials are quoted relative to the Ag/AgCl reference electrode and studies were carried out at room temperature of $18 \text{ }^\circ\text{C}$.

4.3. Synthesis

$\text{K}_8[\gamma\text{-SiW}_{10}\text{O}_{36}]\cdot 12\text{H}_2\text{O}$ (0.33 g, 0.11 mmol) was added to a 50 mL wide-necked conical flask containing 15 mL of an aqueous 0.01 M HNO_3 solution (pH 2.0). After 5 min of vigorous stirring, $[\text{Mn}_3\text{O}(\text{OAc})_6(\text{py})_3] \text{ py}$ (0.1 g, 0.11 mmol) was added to the reaction mixture and allowed to stir vigorously for a further 10 min, after which time the mixture was centrifuged to remove a small amount of unwanted brown-colored precipitate. 0.125 g KCl (1 eq.) was added to the resulting filtrate under vigorous stirring and this final mixture was allowed to stir for a further 15 min. The open conical flask (to allow for moderate evaporation) was set aside to crystallize at a thermostatically controlled room temperature of ca. $18 \text{ }^\circ\text{C}$. Upon 7–10 days of standing, striking yellow–brown plate crystals appeared in the mother liquor. High quality crystals could also be obtained by slow solvent diffusion of acetone into the mother liquor. Yield = 0.08 g, 0.0085 mmol, 23.6% based on W.

Elemental analysis for the partially dehydrated material, $\text{K}_{18}[\text{Mn}^{\text{II}}_2\{\text{Mn}^{\text{III}}(\text{H}_2\text{O})_5\text{Mn}^{\text{III}}_3(\text{H}_2\text{O})(\text{B-}\beta\text{-SiW}_9\text{O}_{34})(\text{B-}\beta\text{-SiW}_6\text{O}_{26})\}_2]\cdot 8\text{H}_2\text{O}$, $\text{H}_{40}\text{K}_{18}\text{Mn}_{10}\text{O}_{140}\text{Si}_4\text{W}_{30}$ (**6**) FW = $9160.76 \text{ g mol}^{-1}$ (partial solvent water loss), calculated values (found values in brackets)%: Mn: 6.00 (5.97), W: 60.24 (59.5), K: 7.66 (7.21). TGA water loss from 25 to $300 \text{ }^\circ\text{C}$, calculated (found)%: 6.14 (6.56). Characteristic FT-IR-bands (cm^{-1}): 3520 (br), 1608 (s), 1534 (s), 1484 (s), 1004 (w), 962 (s), 657 (s), 525 (s). UV-bands, (λ (nm), ϵ ($\text{M}^{-1} \text{ cm}^{-1}$)): 552 (2.21), 355 (3.66).

4.4. Crystallographic analysis

X-ray diffraction structure analysis and crystallographic data: suitable single crystals of **1** were selected and mounted onto the end of a thin glass fibre using Fomblin oil. X-ray diffraction intensity data for compound **1** was measured on an Oxford Diffraction Gemini Ultra with an ATLAS CCD detector [$\lambda(\text{Mo K}\alpha) = 0.71073 \text{ \AA}$] at 150 K. Data reduction was performed using the CRYSDIS software package and structure solution and refinement was carried out using SHELXS-97 [38] and SHELXL-97 [39] via WINGX [40]. Corrections for incident and diffracted beam absorption effects were applied using analytical numeric absorption correction using a multifaceted crystal model [41]. Further details on the X-ray structural analysis for the title compound are given in Table 1.

The W and Mn metal atom positions are crystallographically well-defined but the solvent molecules and K atoms, because of disorder, are difficult to fully analyze by crystallography alone. Therefore, the final molecular formula has been determined by a combination of elemental analysis, thermogravimetric analysis, and crystallography.

Complex **1**: $\text{H}_{64}\text{K}_{18}\text{Mn}_{10}\text{O}_{152}\text{Si}_4\text{W}_{30}$, $M_r = 9380.0 \text{ g mol}^{-1}$; yellow–brown plate crystal: $0.40 \times 0.27 \times 0.03 \text{ mm}^3$; monoclinic space group, $P2_1/c$, $a = 27.8363(6)$, $b = 12.5815(2)$, $c = 22.7819(4) \text{ \AA}$. $\alpha = 90^\circ$, $\beta = 107.580(3)^\circ$, $\gamma = 90^\circ$. $V = 7606.1(2) \text{ \AA}^3$, $Z = 2$, $T = 150 \text{ K}$, $\rho_{\text{calc}} = 4.095 \text{ mg/m}^3$, $\mu(\text{Mo K}\alpha) = 24.015 \text{ mm}^{-1}$, 32618 reflections measured, 13890 unique ($R_{\text{int}} = 0.0516$) which were used in all calculations; structure solution and refinement were performed using WINGX [3]. Final $R_1 = 0.0516$, and $wR_2 = 0.1305$ (all data).

Table 1

Crystal data and structure refinement for the title compound, $K_{18}[Mn^{III}_2\{Mn^{II}(-H_2O)_5Mn^{III}_3(H_2O)(B-\beta-SiW_9O_{34})(B-\beta-SiW_6O_{26})_2\}_2] \cdot 20H_2O$.

Empirical formula	$H_{64}K_{18}Mn_{10}O_{152}Si_4W_{30}$
Formula weight	9380.0
Temperature (K)	150(2)
Wavelength (Å)	0.71073
Crystal system	Monoclinic
Space group	$P2_1/c$
<i>Unit cell dimensions</i>	
<i>a</i> (Å)	27.8363(6)
<i>b</i> (Å)	12.5815(2)
<i>c</i> (Å)	22.7819(4)
α (°)	90
β (°)	107.580(3)
γ (°)	90
Volume (Å ³)	7606.1(2)
<i>Z</i>	2
D_{calc} (mg/m ³)	4.095
Absorption coefficient (mm ⁻¹)	24.015
$F(0\ 0\ 0)$	8296
Crystal size (mm)	0.40 × 0.27 × 0.03
θ Range (°)	3.20–25.50
Limiting indices	$-33 \leq h \leq 33$, $-14 \leq k \leq 15$, $-27 \leq l \leq 27$
Reflections collected/unique	32618/13890 [$R_{int} = 0.0516$]
Unique observed reflections	9116
Completeness to $\theta = 25.50^\circ$	98.0%
Absorption correction	Analytical
Maximum and minimum transmission	0.565 and 0.038
Refinement method	Full-matrix least-squares on F^2
Data/restraints/parameters	13890/0/987
Goodness-of-fit on F^2	0.932
Final <i>R</i> indices [$I > 2\sigma(I)$]	$R_1^a = 0.0516$, $wR_2^a = 0.1305$
<i>R</i> indices (all data)	$R_1^a = 0.0847$, $wR_2^a = 0.1413$
Extinction coefficient	None
Largest difference in peak and hole (e Å ⁻³)	3.231 and –2.580

$$^a R_1 = \sum ||F_o| - |F_c|| / \sum |F_o|; wR_2 = \sum [w(F_o^2 - F_c^2)^2] / \sum [w(F_o^2)^2]^{1/2}.$$

Table 2

Mn–O bond lengths (in Å) from the truncated cubane core unit of $[Mn^{II}_2\{Mn^{II}(H_2O)_5Mn^{III}_3(H_2O)(B-\beta-SiW_9O_{34})(B-\beta-SiW_6O_{26})_2\}]^{18-}$ **1a**.

Bond	Distance (Å)
Mn(2)–O(39) _{eq}	1.916(8)
Mn(2)–O(40) _{eq}	1.851(8)
Mn(2)–O(4) _{eq}	1.929(8)
Mn(2)–O(2) _{eq}	1.998(8)
av. Mn(2)–O _{eq}	1.924(8)
Mn(3)–O(3) _{eq}	1.926(4)
Mn(3)–O(39) _{eq}	1.933(8)
Mn(3)–O(30) _{eq}	1.938(8)
Mn(3)–O(6) _{eq}	1.927(9)
av. Mn(3)–O _{eq}	1.931(9)
Mn(4)–O(30) _{eq}	2.001(8)
Mn(4)–O(7) _{eq}	1.861(9)
Mn(4)–O(1) _{eq}	1.953(8)
Mn(4)–O(37) _{eq}	1.917(8)
av. Mn(4)–O _{eq}	1.933(9)
<i>Short axial bond</i>	
Mn(2)–O(5) _{ax}	2.112(8)
Mn(3)–O(2) _{ax}	2.128(8)
Mn(4)–O(29) _{ax}	2.048(8)
av. Mn–O _{ax}	2.096(8)
<i>Long axial bond</i>	
Mn(2)–O(5) _{ax2}	2.283(8)
Mn(3)–O(63) _{ax2}	2.240(8)
Mn(4)–O(2) _{ax2}	2.254(8)
av. Mn–O _{ax2}	2.259(8)

Acknowledgements

We thank the EPSRC, BP, WestCHEM, The Leverhulme Trust, and the University of Glasgow for funding and Michael Beglan for assistance with FAAS analysis.

Appendix A. Supplementary material

CSD 422027 contains the supplementary crystallographic data for this paper. The data can be obtained free of charge from Fachinformationszentrum Karlsruhe, 76344 Eggenstein-Leopoldshafen, Germany (http://www.fiz-karlsruhe.de/request_for_deposited_data.html). Supplementary data associated with this article can be found, in the online version, at [doi:10.1016/j.ica.2010.07.020](https://doi.org/10.1016/j.ica.2010.07.020).

References

- [1] M.T. Pope, A. Müller, *Angew. Chem., Int. Ed.* 30 (1991) 34.
- [2] (a) D.-L. Long, E. Burkholder, L. Cronin, *Chem. Soc. Rev.* 36 (2007) 105; (b) D.-L. Long, R. Tsunashima, *Angew. Chem., Int. Ed.* 49 (2010) 1736.
- [3] A. Müller, F. Peters, M.T. Pope, D. Gatteschi, *Chem. Rev.* 98 (1998) 239.
- [4] U. Kortz, A. Müller, J. van Slageren, J. Schnack, N.S. Dalal, M. Dressel, *Coord. Chem. Rev.* 253 (2009) 2315.
- [5] H. Yanagie, A. Ogata, S. Mitsui, T. Hisa, T. Yamase, M. Eriguchi, *Biomed. Pharmacother.* 60 (2006) 349.
- [6] C. Ritchie, A. Ferguson, H. Nojiri, H.N. Miras, Y.F. Song, D.-L. Long, E. Burkholder, M. Murrie, P. Kögerler, E.K. Brechin, L. Cronin, *Angew. Chem., Int. Ed.* 47 (2008) 5609.
- [7] L.M. Rodriguez-Albelo, A.R. Ruiz-Salvador, A. Sampieri, D.W. Lewis, A. Gomez, B. Nohra, P. Mialane, J. Marrot, F. Sécheresse, C. Mellot-Draznieks, R.N. Biboum, B. Keita, L. Nadjo, A. Dolbecq, *J. Am. Chem. Soc.* 131 (2009) 16078.
- [8] Y. Yamamoto, S. Hatanaka, K. Tsuji, K. Tsuneyama, R. Ohnishi, H. Imai, Y. Kamiya, T. Okuhara, *Appl. Catal. A-Gen.* 344 (2008) 55.
- [9] S.G. Mitchell, C. Streb, H.N. Miras, T. Boyd, D.-L. Long, L. Cronin, *Nat. Chem.* 2 (2010) 308.
- [10] R. Tsunashima, D.-L. Long, H.N. Miras, D. Gabb, C.P. Pradeep, L. Cronin, *Angew. Chem., Int. Ed.* 49 (2010) 113.
- [11] M. Prinz, A.F. Takacs, J. Schnack, I. Balasz, E. Burzo, U. Kortz, K. Kuepper, M. Neumann, *J. Appl. Phys.* 8 (2006) 99.
- [12] I.M. Mbomekalle, B. Keita, L. Nadjo, P. Berthet, W.A. Neiwert, C.L. Hill, M.D. Ritorto, T.M. Anderson, *Dalton Trans.* 13 (2003) 2646.
- [13] S.G. Mitchell, C. Ritchie, D.-L. Long, L. Cronin, *Dalton Trans.* 11 (2008) 1415.
- [14] N.H. Nsouli, A.H. Ismail, I.S. Helgadottir, M.H. Dickman, J.M. Clemente-Juan, U. Kortz, *Inorg. Chem.* 48 (2009) 5884.
- [15] J. Canny, A. Tézé, R. Thouvenot, G. Hervé, *Inorg. Chem.* 25 (1986) 2114.
- [16] D. Gatteschi, R. Sessoli, *Angew. Chem., Int. Ed.* 42 (2003) 268.
- [17] E. Coronado, A. Forment-Aliaga, A. Gaita-Arino, C. Gimenez-Saiz, F.M. Romero, W. Wernsdorfer, *Angew. Chem., Int. Ed.* 43 (2004) 6152.
- [18] T.J.R. Weakley, H.T. Evans, J.S. Showell, G.F. Tourné, C.M. Tourné, *J. Chem. Soc., Chem. Commun.* 4 (1973) 139.
- [19] N. Laronze, J. Marrot, G. Hervé, *Inorg. Chem.* 42 (2003) 5857.
- [20] D. Drewes, E.M. Limanski, B. Krebs, *Eur. J. Inorg. Chem.* 8 (2005) 1542.
- [21] W.H. Knoch, P.J. Domaille, R.L. Harlow, *Inorg. Chem.* 25 (1986) 1577.
- [22] C. Ritchie, F.Y. Li, C.P. Pradeep, D.-L. Long, L. Xu, L. Cronin, *Dalton Trans.* 33 (2009) 6483.
- [23] S.T. Zheng, J. Zhang, J.M. Clemente-Juan, D.Q. Yuan, G.Y. Yang, *Angew. Chem., Int. Ed.* 48 (2009) 7176.
- [24] M.A. Aldamen, J.M. Clemente-Juan, E. Coronado, C. Martí-Gastaldo, A. Gaita-Arino, *J. Am. Chem. Soc.* 130 (2008) 8874.
- [25] B.S. Bassil, U. Kortz, A.S. Tigan, J.M. Clemente-Juan, B. Keita, P. de Oliveira, L. Nadjo, *Inorg. Chem.* 44 (2005) 9360.
- [26] U. Kortz, S. Nellutla, A.C. Stowe, N.S. Dalal, U. Rauwald, W. Danquah, D. Ravot, *Inorg. Chem.* 43 (2004) 2308.
- [27] C. Ritchie, C. Streb, J. Thiel, S.G. Mitchell, H.N. Miras, D.-L. Long, T. Boyd, R.D. Peacock, T. McGlone, L. Cronin, *Angew. Chem., Int. Ed.* 47 (2008) 6881.
- [28] T.D. Pfister, A.Y. Mirarefi, A.J. Gengenbach, X. Zhao, C. Danstrom, N. Conatser, Y.G. Gao, H. Robinson, C.F. Zukoski, A.H.J. Wang, Y. Lu, *J. Biol. Inorg. Chem.* 12 (2007) 126.
- [29] R. Brimblecombe, D.R.J. Kolling, A.M. Bond, G.C. Dismukes, G.F. Swiegers, L. Spiccia, *Inorg. Chem.* 48 (2009) 7269.
- [30] K.N. Ferreira, T.M. Iverson, K. Maghlaoui, J. Barber, S. Iwata, *Science* 303 (2004) 1831.
- [31] Y.V. Geletii, C. Besson, Y. Hou, Q. Yin, D.G. Musaev, D. Quiñero, R. Cao, K.I. Hardcastle, A. Proust, P. Kögerler, C.L. Hill, *J. Am. Chem. Soc.* 131 (47) (2009) 17360.
- [32] Q. Yin, J.M. Tan, C. Besson, Y.V. Geletii, D.G. Musaev, A.E. Kuznetsov, Z. Luo, K.I. Hardcastle, C.L. Hill, *Science* 328 (2010) 342.
- [33] A. Tézé, G. Hervé, A.P. Ginsberg (Eds.), *Inorganic Synthesis*, John Wiley & Sons, 1990.
- [34] (a) L.H. Bi, E.-B. Wang, J. Peng, R.D. Huang, L. Xu, C.W. Hu, *Inorg. Chem.* 39 (2000) 671;

- (b) S. Mitchell, S. Khanra, H.N. Miras, T. Boyd, D.-L. Long, L. Cronin, *Chem. Commun.* (2009) 2712;
(c) J. Yan, D.-L. Long, H.N. Miras, L. Cronin, *Inorg. Chem.* 49 (2010) 1819.
- [35] (a) I.M. Mbomekalle, B. Keita, L. Nadjjo, P. Berthet, W.A. Neiwert, C.L. Hill, M.D. Ritorto, T.M. Anderson, *Dalton Trans.* (2003) 2646;
(b) B.S. Bassil, M.H. Dickman, M. Reicke, U. Kortz, B. Keita, L. Nadjjo, *Dalton Trans.* (2006) 4253;
(c) T. Boyd, S.G. Mitchell, H.N. Miras, D.-L. Long, L. Cronin, *Dalton Trans.* (2010), doi:10.1039/c002633f.
- [36] J. Liw, F. Ortega, P. Sethuraman, D.E. Katsoulis, C.E. Costello, M.T. Pope, *J. Chem. Soc., Dalton Trans.* (1992) 1901.
- [37] (a) M. Bosing, A. Noh, I. Loose, B. Krebs, *J. Am. Chem. Soc.* 120 (1998) 7252;
(b) B. Keita, I.M. Mbomekalle, Y.W. Lu, L. Nadjjo, P. Berthet, T.M. Anderson, C.L. Hill, *Eur. J. Inorg. Chem.* (2004) 3462;
(c) A. Tézé, G. Hervé, *Inorg. Synth.* 27 (1990) 85.
- [38] G.M. Sheldrick, Phase annealing in SHELX-90: direct methods for larger structures, *Acta Crystallogr., Sect. A* 46 (1990) 467–473.
- [39] G.M. Sheldrick, A short history of SHELX, *Acta Crystallogr., Sect. A* 64 (2008) 112–122.
- [40] L.J. Farrugia, WINGX suite for small-molecule single-crystal crystallography, *J. Appl. Cryst.* 32 (1999) 837–838.
- [41] R.C. Clark, J.S. Reid, *Acta Crystallogr., Sect. A* 51 (1995) 887–897.